Supplement to von Hagke et al. - Front. Earth Sci. | doi: 10.3389/feart.2019.00018

The effect of obliquity of slip in normal faults on distribution of open fractures

1. Material Properties

1.1 Density

To determine the density of the powder, the material has to be sieved from a height >30 cm (van Gent et al., 2010). Based on five measurements, we determined a density of 898 kg/m³ with a standard deviation of 0.78 %. These values are slightly higher than the values obtained by van Gent et al. (2010) and Holland et al. (2006), who measured 732 and 864 kg/m³, respectively, for hemihydrate powder of a different manufacturer. The density of the sand-powder mixture is 1404 kg/m³ with a standard deviation of 0.54%.

1.2 Shear tests

For shear cell measurements, we use a modified Jenike shear cell. For normal consolidation a standard shear experiment with constant vertical stress is used, where after a certain shear strain, the shear stress reaches a steady-state slope. The shear stress value at which this stead-state slope is reached is used as the failure locus. For over-consolidation experiments, the sample is vertically pre-compacted. This results in a stronger sample, caused by reorganization of the grain fabric and a lowering of porosity(Schweiger and Zimmermann, 1999). The loaded sample is then sheared to establish a normally consolidated failure locus. Having reached the failure locus, the shear force is relaxed and the vertical load is reduced. Reapplying horizontal load yields an over-consolidated shear failure locus. Reduction of vertical loading can be repeated, allowing for multiple over-consolidated shear tests in one sample (Fig. S1). Each measurement cycle shows a peak in shear stress and a consecutive dynamic shear stress. Peak stress is the static stress needed to (re-)activate the shear plane, while the dynamic shear stress is the stress needed to keep the shear plane sliding. The peak stresses and their respective normal stresses are used as failure loci.

To visualize shearing within the sample, we implemented vertical markers of colored powder, and we excavated shear planes from the sheared hemihydrate sample, using a vacuum cleaner (Fig. S1C). These analyses show deformation occurs along multiple discrete shear planes separating areas of macroscopically homogenous simple shear. The shear planes transect the entire sample and form within the powder cake i.e. not at the powder-shear cell interface.

For normal consolidation experiments, shear test yield a cohesion of 34.5 Pa and an angle of internal friction of 36°. For over-consolidated powder, cohesion is 131.7 Pa, and the angle of internal friction is 40° (Fig. S2). These values differ from the values obtained by Holland et al. (2006) and van Gent et al. (2010) for other hemihydrate powders. Holland et al. (2006) determined the failure loci from over-consolidated measurements. These failure loci produced a convex critical failure envelope, indicating a cohesion of 62 Pa. van Gent et al. (2010) performed both normal and over-consolidation experiments. From over-consolidated measurements, they found that the cohesion of hemihydrate increases linearly with pre-compaction, while the coefficient of internal friction remains roughly constant (c. 0.6). van Gent et al. (2010) measured a cohesion of 40 Pa for uncompacted hemihydrate powder, which is similar to 34.5 Pa of this study. These findings underscore the necessity to perform individual material characterization tests for different hemihydrate products.

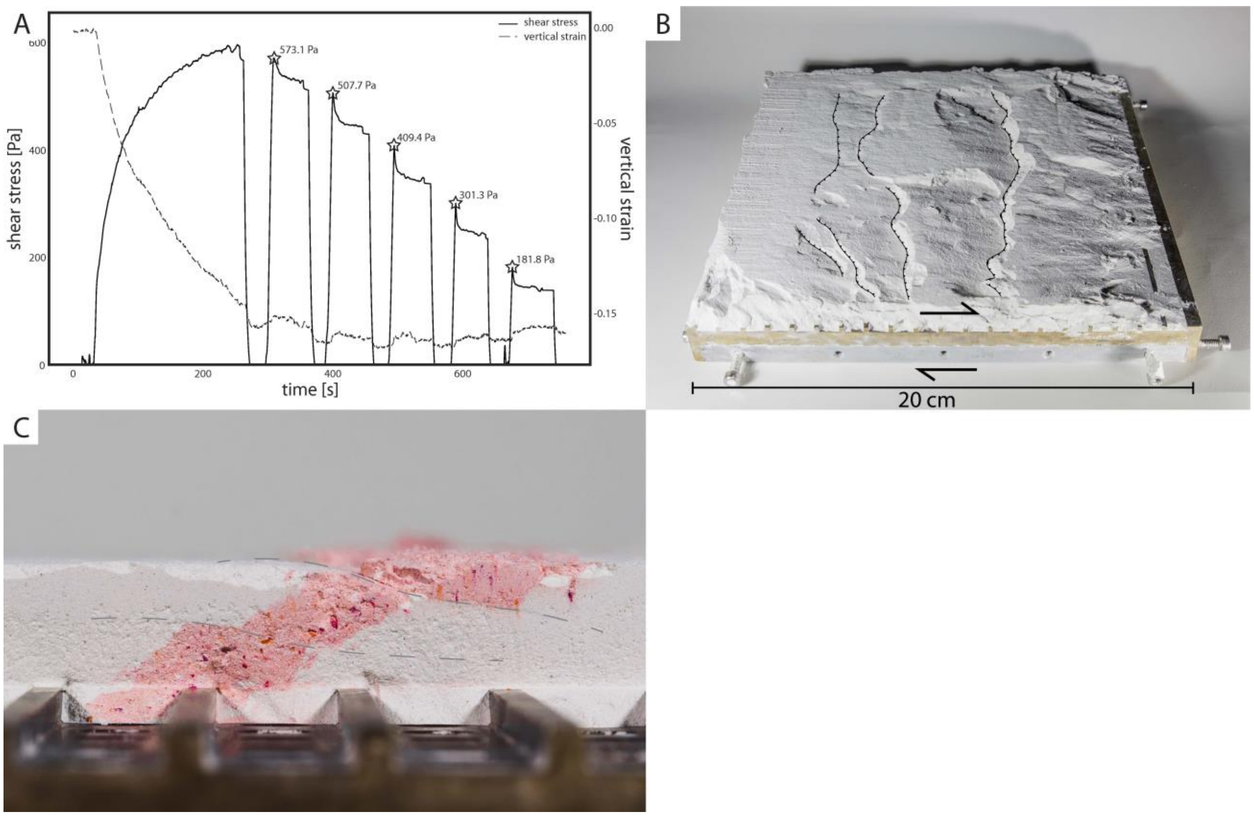

Fig. S1: Shear Tests. A: Typical example of a shear test with overconsolidated hemihydrate powder. Time (or cumulative shear strain) is plotted against shear stress. With increasing strain, shear stress increases. After failure, peak stresses drop; peak stresses for different cycles of loading correspond to the critical shear stresses at brittle failure. Reduction of initial vertical stress in five steps results in five peak shear stress data points. B: Exhumed shear plane after shear cell measurement under normal consolidation. The sample has reached steady state slip, and multiple shear planes developed, indicated with black lines. C: Sheared vertical marker in shear cell experiment. The marker shows both the discrete shear planes but also distributed simple shear deformation. Shear planes are indicated as dashed lines.

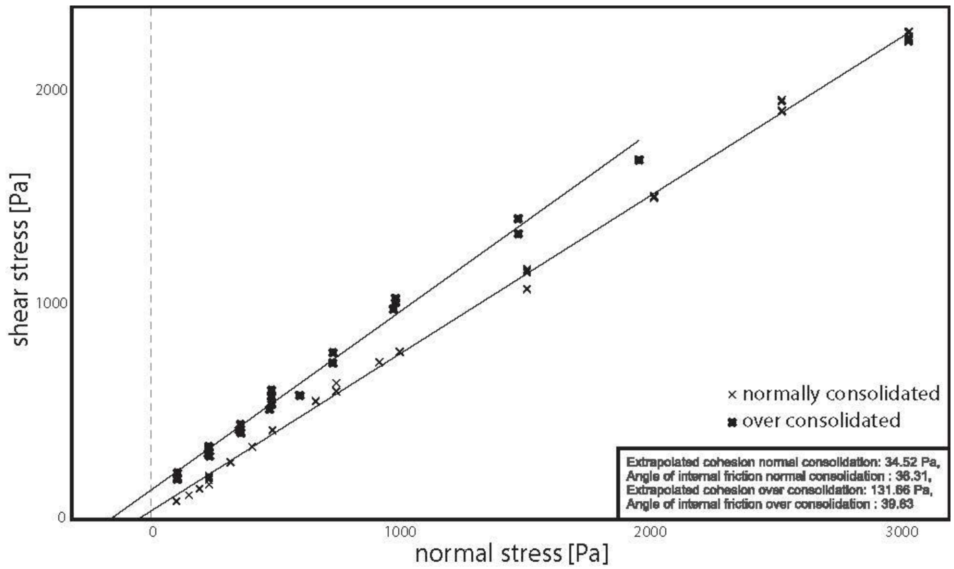

Fig. S2: Mohr space representation of shear cell measurements for normal consolidation and over-consolidated experiments

1.3 Tensile strength

To characterize the influence of initial overburden on tensile strength, in total 13 measurements were carried for overburden stresses in the range of 72 Pa – 650 Pa. Tensile strength of the hemihydrate powder increases linearly with increasing overburden. The empirical relationship is

$$T_0^{hemihydrate} = 0.058 * \sigma_n + 15.67$$

The extrapolated tensile strength of uncompressed hemihydrate powder is therefore 15.7 Pa. A linear increase of tensile strength with overburden is consistent with findings of Holland et al. (2006) and van Gent et al. (2010). Tensile strength for uncompacted hemihydrate in this study falls between the values derived by van Gent (2006) and Holland et al. (2006), who obtained values of 9 Pa and 47 Pa, respectively.

1.4 Material characterization of hemihydrate-sand mixtures

We tested different hemihydrate-sand mixtures to be able to perform models with materials with less shear strength. A hemihydrate-sand mixing ratio of 1:10 proved to be much weaker than pure hemihydrate, while still being able to form vertical cliffs. For this material, a tensile strength of 2.4 Pa, and a true cohesion of 4.8 Pa was determined.

2. Scaling

In order to resemble observed geologic structures, the three fundamental physical quantities length, mass and time need to be scaled in analog experiments (Cloos, 1929;Hubbert, 1937). Based on these, all other quantities such as stress, strain or forces can be described. Our experiments are time independent and gravitational acceleration is the same in nature and model. Length ratio λ can be determined from the ratio of stresses and strength σ and the ratio of density δ (Hubbert, 1937): $\lambda = \sigma / \delta$.

To determine the stress and density ratios, we use values measured on rocks in Iceland. We calculate density and cohesion ratios for different rock types, in particular Tholeiitic and Olivine basalt and scoria (Gunnarsson, 2008), as well as weak and strong hyaloclastite (Friese, 2008). Different relationships between rock strength and cohesion have been proposed:

$$c = \frac{\sigma_C}{2}\left(\frac{1-\sin(\phi)}{\cos(\phi)}\right) \qquad (1)$$

where c denotes cohesion, σ_C is uniaxial compressive strength, and ϕ is the angle of internal friction (Miedema and Zijsling, 2012)

$$c = \sqrt{3\sigma_T} \qquad (2)$$

where σ_T denotes tensile strength (Madland et al., 2002).

$$c = 1.82 * \sigma_T \qquad (3)$$

which is an empirical relationship based on laboratory tests of 35 sets of rock specimens (Sivakugan et al., 2014). Eventually Sivakugan et al. (2014) derive cohesion from σ_C and σ_T as

$$c = \frac{0.5\sigma_C\sigma_T}{\sqrt{(\sigma_C-3\sigma_T)\sigma_T}} \quad (4),$$

which yields the same values as (1)

Similarly, Sivakugan et al. (2014) derive the angle of internal friction from σ_C and σ_T as

$$\phi = sin^{-1}\left(\frac{\sigma_C-4\sigma_T}{\sigma_C-2\sigma_T}\right) \quad (5)$$

Cohesion values are all comparable and differ by a maximum of about 20% (Table S1). Maximum and minimum values are obtained using equations (1) and (2), respectively. Corresponding length ratios λ_{C1} and λ_{C2} vary by approximately 20 % or less. Length ratios for different rock types vary by an order of magnitude, as a result of similar variation in cohesion. This variation is expected, as the tested rock specimens show different degrees of weathering and internal fracturing (Gunnarsson, 2008). For our models this implies that 1 cm of model material can be translated to 2500 to 2900 m of intact or 300 to 500 m of weathered basalt or scoria, respectively. Additionally, differences between rock strength and bulk rock strength of two orders of magnitude are expected (Schultz, 1996). 1 cm in our models thus represents approximately 50 m of rock column. The 1o10 mixture is 6.6 times weaker than the hemihydrate powder. Using the same length scale as for basalts, it represents scoria or weak hyaloclastite. We note that for hyaloclastite σ_C was not determined. We used the relationship between σ_C / σ_T, which commonly ranges between c. 4 and 15.

Rock properties obtained in Iceland may be compared to typical values obtained in other basalts. An average basalt density of 2.67 g/cm³ was determined based on measurements of 1,600 samples from Hawaiian basalt (Moore, 2001). This value is similar to values obtained in Icelandic basalts as they were measured in subaerial lavas, pillows and hyaloclastites similar to those observed in Iceland. Cohesion of intact basalt, ranges between 32 MPa (Birch, 1966) and 66 MPa (Schultz, 1995). These values are higher than the ones obtained in basalts on Iceland. Cohesion of 66 MP would result in a length ratio of 1/700 instead of 1/290. All scaling relationships using the different cohesion values are provided in Table S1

Table S1: Scaling. Length ratio λ calculated for different rock types found on Iceland. Cohesion can be determined from compressive and tensile strengths following different approaches (see text). Cohesion values C1 – C4 reproduce within 20 % error at max. ρ is rock density, σC denotec uniaxial compressive strength, σT denotes tensile strength, ϕ is angle of internal friction, δ is density ratio. σ is strength ratio as calculated from max and min cohesion values. λ are respective length ratios from nature to model, indicating how many meters of rock column corresponds to 1 cm of the model.

Natural Examples

	ρ [kg/m³]	σT [MPa]	σC [MPa]	φ [°]	C1 [MPa]	C 2 [MPa]	C 3 [MPa]	C 4 [MPa]	σC / σT	δ	σ (C1)	σ (C2)	λ (C1)	λ (C2)
Tholeiite Basalt 1	2800	193	13	57.6	28.0	22.5	23.7	28.0	14.8	3118.0	0.89	0.72	286.8	230.3
Tholeiite Basalt 2	2500	30	3.7	42.3	6.6	6.4	6.7	6.6	8.1	2784.0	0.21	0.20	76.0	73.4
Olivine Basalt 1	2900	168	12	56.4	25.3	20.8	21.8	25.3	14.0	3229.4	0.81	0.66	250.2	205.3
Olivine Basalt 2	2300	24.5	2.2	51.4	4.3	3.8	4.0	4.3	11.1	2561.2	0.14	0.12	53.5	47.5
Scoria 1	2200	23	4.7	18.0	8.4	8.1	8.6	8.4	4.9	2449.9	0.27	0.26	108.8	106.0
Scoria 2	2600	16	1.7	46.9	3.2	2.9	3.1	3.2	9.4	2895.3	0.10	0.09	34.8	32.4
weak Hyaloclastite	1400	4	0.8	19.5	1.4	1.4	1.5	1.4	5.0	1559.0	0.05	0.04	28.9	28.4
strong Hyaloclastite	2200	40	2.8	56.8	6.0	4.8	5.1	6.0	14.3	2449.9	0.19	0.15	77.5	63.1

Analog Materials

	ρ [kg/m³]	σT [Pa]	C ([Pa]
Hemihydrate Powder	0.898	15.68	31.35
1to10Mixture	1.404	2.39	4.78

3. Methods

3.1 quantitative mapping of experiments

We use the ArcGIS and GEORIENT software packages to map and analyze structures at the surface. To quantify dilatancy, we first mapped the area fraction of open gaps by manually tracing open fracture networks in ArcGIS. To determine average dilatancy, we used scanlines with spacing of five mm, oriented normally to the direction of fault movement. We determined wavelength of the structure by visual inspection of the traced fault outlines (Fig. S3). Comparing final and early stages of the models shows the geometry of the final fault is dominated by orientation and location of early fractures. Figure S-4 shows a comparison of the structures in experiments with pure powder and experiments with 1:10 mixture. Images taken after 24 mm displacement of the basement fault.

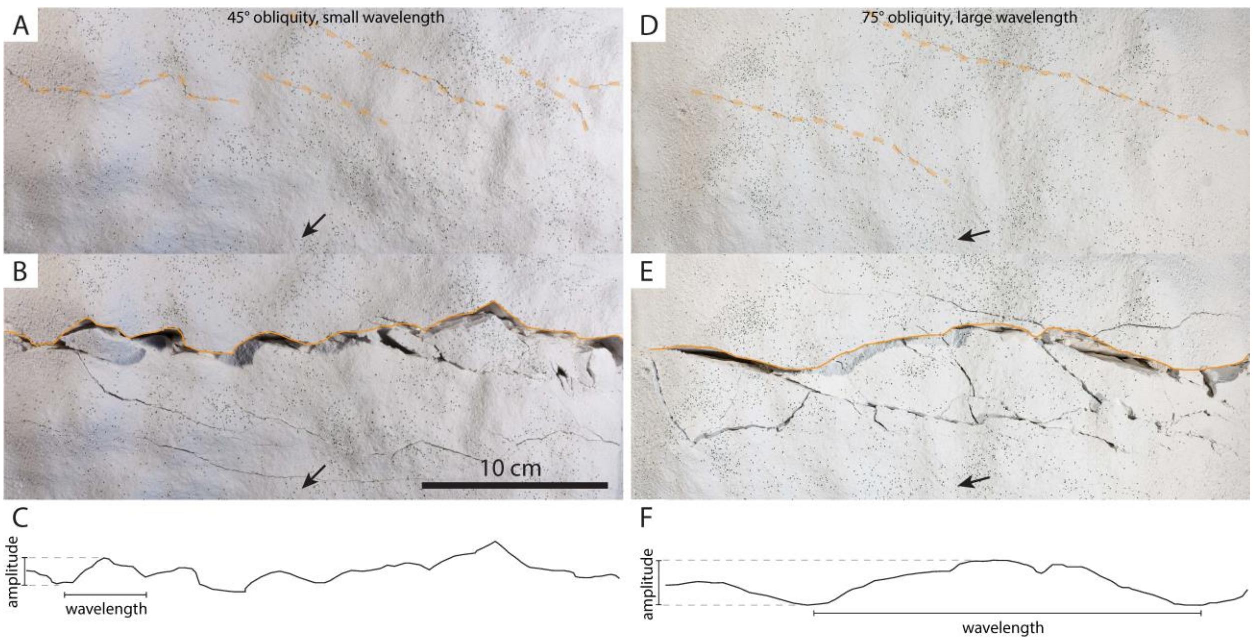

Fig. S3: Influence of early fractures on final fault geometry. A: Experiments at obliquities of 45° and lower. Short en-échelon fractures from, which are later linked to form the main fault. Geometry of the main fault shows a characteristic zig-zag pattern. B: experiments with 60° obliquity and higher. Long R-shears develop, leading to releasing and restraining bends in later stages of the experiment. Early fractures do not necessarily link, but continue accommodating strain during the entire experiment.

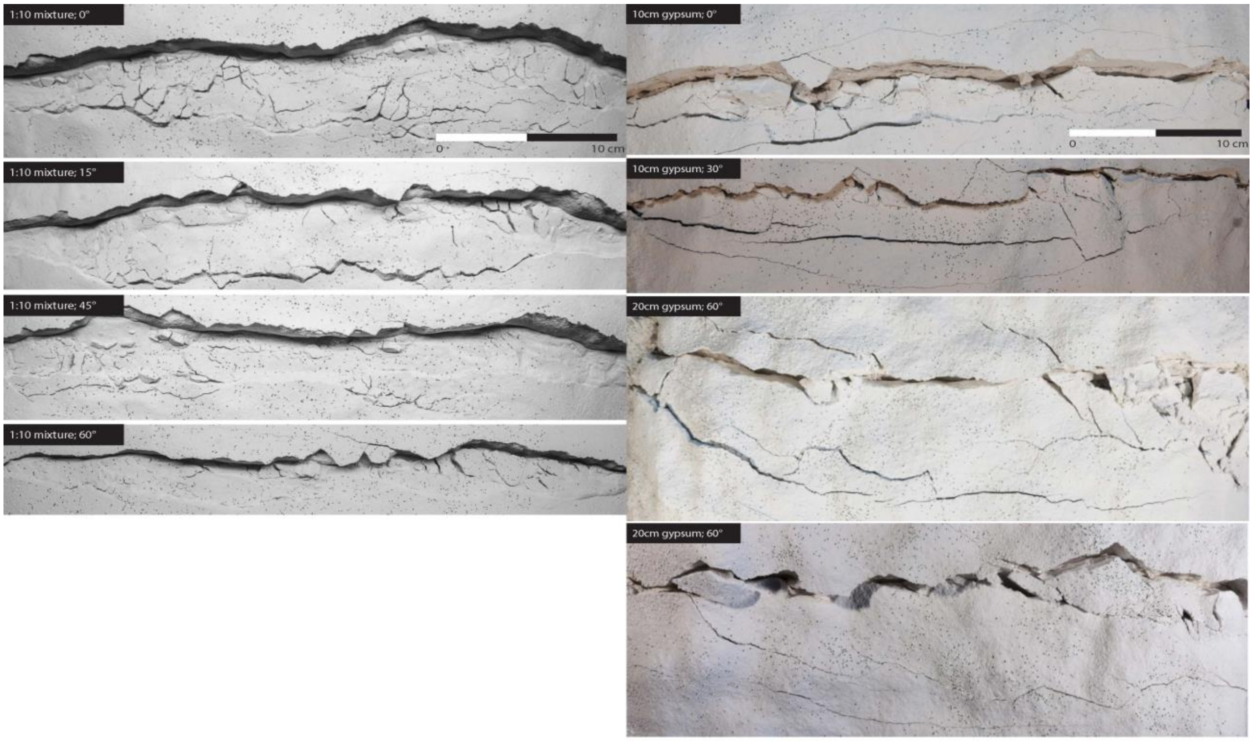

Fig. S4: Comparison of experiments with different material strengths. Left column shows 1to10 mixture experiments, right column shows powder experiments. 1to10mixture experiments show vertical walls, however dilatant fractures are not as deep as compared to powder experiments.

3.1 unmanned aerial vehicles

During the field work, we used three different unmanned aerial vehicles (UAVs) by the manufacturer DJI, the Phantom 4 (12 MP sensor), Phantom 4 Advanced (20 MP sensor) and the Mavic Pro (12 MP sensor) to capture several thousand photographs of the faults. Flying parallel to the faults strike, we took vertical photographs while maintaining a frontal overlap of ~ 70% and ~ 50% sidelap. The photograph sets were processed with the commercial photogrammetry software Agisoft Photoscan, which we use to create a dense point cloud, and a successive digital elevation model (DEM) and orthomosaic. For data extraction, the relative heights are important. Relative measurements are consistent, i.e. 1 m in the field equals 1 m in the DEM. For georeferencing our DEMs we use the GPS positioning data written in the images by the UAVs. In the models, horizontal referencing error is < 3 m; vertical error is approximately 30 m on average. This implies that absolute values above sea level are associated with a relatively large error. However, we only require relative heights within the model, which are accurate. Depending on the size of the photographed areas we captured images at flight altitudes ranging from ~ 30 m for small to ~ 70 m for larger areas. This results in average resolutions of 5 – 15 cm/pixel in the DEMs and 5 – 10 cm/pixel in the orthomosaics. Measurements of graben width, fault strike and angles of obliquity were taken on the DEMs using the ArcGIS software.

4. Depth of failure mode transition

Abe et al. (2011) predict depth of shear failure d_{max} as a function of vertical stress at failure mode transition and density:

$$d_{max} = \frac{\sigma_v^{tr}}{g\rho}$$

and

$$\sigma_v^{tr} = \frac{-\frac{2C}{tan\phi} - T(1 + \frac{1}{\sin\phi})}{1 - \frac{1}{sin\phi}}$$

where C is the cohesion of the material, T is the tensile strength, ϕ is the angle of internal friction and ρ is density.

Gudmundsson (1992) determines depth of shear failure d_{max} from tensile strength and density:

$$d_{max} = \frac{T_0}{g\rho}$$

where T_0 is tensile strength and ρ is density.

5. References

Abe, S., Van Gent, H.W., and Urai, J.L. (2011). DEM Simulation of Normal Faults in cohesive Materials. *Tectonophysics* 512**,** 12-21.

Birch, F. (1966). "Compressibility; elastic constants," in *Handbook of physical constants,* ed. S.P. Clark. Geological Society of America Memoir), 97-173.

Cloos, H. (1929). Künstliche Gebirge. *Natur und Museum. Ed. by Senckenberg Naturforschende Gesellschaft* 5**,** 225-243.

Friese, N. (2008). Brittle tectonics of the Thingvellir and Hengill volcanic systems, Southwest Iceland: field studies and numerical modelling. *Geodinamica Acta* 21**,** 169-185.

Gudmundsson, A. (1992). Formation and growth of normal faults at the divergent plate boundary in Iceland. *Terra Nova* 4**,** 464-471.

Gunnarsson, G.A. (2008). *Rock Mass Characterisation and Reinforcement Strategies for Tunnels in Iceland.* MSc Thesis; Department of Civil Engineering, Technical University of Denmark; Faculty of Civil and Environmental Engineering, University of Iceland.

Holland, M., Urai, J.L., and Martel, S. (2006). The internal structure of fault zones in basaltic sequences. *Earth and Planetary Science Letters* 248**,** 286-300.

Hubbert, M.K. (1937). Theory of scale models as applied to the study of geological structures. *Bulletin of the Geological Society of America* 48**,** 1459-1520.

Madland, M.V., Korsnes, R.I., and Risnes, R. (Year). "Temperature effects in Brazilian, uniaxial and triaxial compressive tests with high porosity chalk", in: *SPE Annual Technical Conference and Exhibition*: Society of Petroleum Engineers).

Miedema, S., and Zijsling, D. (Year). "Hyperbaric Rock Cutting", in: *Proceedings of the ASME 2012 31th International Conference on Ocean, Offshore and Arctic Engineering*).

Moore, J.G. (2001). Density of basalt core from Hilo drill hole, Hawaii. *Journal of Volcanology and Geothermal Research* 112**,** 221-230.

Schultz, R. (1995). Limits on strength and deformation properties of jointed basaltic rock masses. *Rock Mechanics and Rock Engineering* 28**,** 1-15.

Schultz, R.A. (1996). Relative scale and the strength and deformability of rock masses. *Journal of Structural Geology* 18**,** 1139-1149.

Schweiger, A., and Zimmermann, I. (1999). A new approach for the measurement of the tensile strength of powders. *Powder technology* 101**,** 7-15.

Sivakugan, N., Das, B., Lovisa, J., and Patra, C. (2014). Determination of c and φ of rocks from indirect tensile strength and uniaxial compression tests. *International Journal of Geotechnical Engineering* 8**,** 59-65.

Van Gent, H.W., Holland, M., Urai, J.L., and Loosveld, R. (2010). Evolution of fault zones in carbonates with mechanical stratigraphy–Insights from scale models using layered cohesive powder. *Journal of Structural Geology* 32**,** 1375-1391.